



1 **Origin of elemental carbon in snow from Western Siberia**
2 **and northwestern European Russia during winter–spring**
3 **2014, 2015 and 2016**

4
5 **Nikolaos Evangeliou^{1,*}, Vladimir P. Shevchenko², Karl Espen Yttri¹, Sabine**
6 **Eckhardt¹, Espen Sollum¹, Oleg S. Pokrovsky^{3,4}, Vasily O. Kobelev⁵, Vladimir B.**
7 **Korobov⁶, Andrey A. Lobanov⁵, Dina P. Starodymova², Sergey N. Vorobiev⁷,**
8 **Rona L. Thompson¹, Andreas Stohl¹**

9
10 ¹ NILU - Norwegian Institute for Air Research, Department of Atmospheric and Climate
11 Research (ATMOS), Kjeller, Norway.

12 ² Shirshov Institute of Oceanology, Russian Academy of Sciences, Nakhimovsky prospect 36,
13 117997 Moscow, Russia.

14 ³ Geosciences Environment Toulouse, UMR 5563 CNRS, University of Toulouse, 14 Avenue
15 Edouard Belin, 31400, Toulouse, France.

16 ⁴ N. Laverov Federal Center for Integrated Arctic Research, Russian Academy of Science,
17 Sadovaya street, 3, 163000, Arkhangelsk, Russia.

18 ⁵ Arctic Research Center of the Yamalo-Nenets autonomous district, Vos'moy proezd, NZIA
19 building, 629730, Nadym, Yamalo-Nenets autonomous district, Russia.

20 ⁶ North-Western Branch of Shirshov Institute of Oceanology, Russian Academy of Sciences,
21 Naberezhnaya Severnoy Dviny 112/3, 163061, Arkhangelsk, Russia.

22 ⁷ BIO-GEO-CLIM Laboratory, Tomsk State University, 36 Prospect Lenina, 634050, Tomsk,
23 Russia.

24

25 *Correspondence to: N. Evangeliou, NILU - Norwegian Institute for Air Research,
26 Department of Atmospheric and Climate Research (ATMOS), Kjeller, Norway
27 (Nikolaos.Evangeliou@nilu.no)

28

29 **Abstract**

30 Short-lived climate forcers have been proven important both for the climate and human
31 health. In particular, black carbon (BC) is an important climate forcer both as an aerosol and
32 when deposited on snow and ice surface, because of its strong light absorption. This paper
33 presents measurements of elemental carbon (EC; a measurement-based definition of BC) in
34 snow collected from Western Siberia and northwestern European Russia during 2014, 2015
35 and 2016. The Russian Arctic is of great interest to the scientific community due to the large
36 uncertainty of emission sources there. We have determined the major contributing sources of
37 BC in snow in Western Siberia and northwestern European Russia using a Lagrangian
38 atmospheric transport model. For the first time, we use a recently developed feature that
39 calculates deposition in backwards (so-called retroplume) simulations allowing estimation of
40 the specific locations of sources that contribute to the deposited mass.

41 EC was found in higher levels compared to previously reported concentrations and it
42 was highly variable depending on the sampling location. Modelled BC was in good agreement
43 ($R = 0.53 - 0.83$) with measured EC. However, a systematic region-specific model
44 underestimation was found. For EC sampled in northwestern European Russia the
45 underestimation by the model was smaller ($> -100\%$). In this region, the major sources were
46 transportation activities and domestic combustion in Finland. When sampling shifted to
47 Western Siberia, the model underestimation was more significant ($< -100\%$). There, the
48 sources included emissions from gas flaring as a major contributor to snow BC. The accuracy
49 of the model calculations was also evaluated using two independent datasets of BC
50 measurements in snow covering the entire Arctic. The model reproduced snow BC
51 concentrations quite accurately, although small discrepancies occurred mainly for samples
52 collected in springtime. Nevertheless, EC concentrations in snow presented here are about
53 20% lower than previously reported ones in Western Siberia and northwestern European
54 Russia.

55



56 **1 Introduction**

57 Black carbon (BC) is the most strongly light-absorbing component of the atmospheric
58 aerosol and is formed by the incomplete combustion of fossil fuels, biofuels, and biomass
59 (Bond et al., 2013). It is emitted directly into the atmosphere in the form of fine particles. BC
60 is a major component of “soot”, a complex light-absorbing mixture that also contains organic
61 carbon (OC) (Bond et al., 2004). Combustion sources emitting BC include open biomass
62 burning (forest, savanna, agricultural burning), residential biofuel combustion, diesel engines
63 for transportation or industrial use, industrial processes and power generation, or residential
64 coal combustion (Liu et al., 2011; Wang et al., 2011).

65 The main reasons why BC is important on a global perspective are its impacts on human
66 health and on climate. As a component of the fine particulate matter (PM_{2.5}), it is associated
67 with negative health impacts, including premature mortality (Lelieveld et al., 2015; Turner et
68 al., 2005). It also absorbs solar radiation, has a significant impact on cloud formation and,
69 when deposited on ice and snow, it absorbs radiation there and accelerates melting (Hansen
70 and Nazarenko, 2004). BC has a lifetime that can be as long as 9–16 days (Bond et al., 2013).
71 After its emission, BC can travel over long distances (Forster et al., 2001; Stohl et al., 2006)
72 and reach remote areas such as the Arctic. Arctic land areas are covered by snow in winter
73 and spring, while the Arctic Ocean is partly covered by ice. Sea ice has a much higher albedo
74 (≈ 0.5 – 0.7) compared to the surrounding ocean (≈ 0.06), thus BC deposited on sea ice reduces
75 the heat uptake of the ocean. Snow has an even higher albedo than sea ice and can reflect as
76 much as 90% of the incoming solar radiation (Brandt et al., 2005; Singh and Haritashya,
77 2011).

78 Hegg et al. (2009) reported that snow in the Arctic often contains BC at concentrations
79 between 1 and 30 ppb, which can cause a snow albedo reduction of 1–3% in fresh snow and
80 another 3–9% as snow ages and BC becomes more concentrated near the surface (Clarke and
81 Noone, 1985). This solar radiation reflecting capacity of snow insulates the sea ice, maintains
82 cold temperatures and delays ice melt in summertime. After the snow begins to melt and
83 because shallow melt ponds have an albedo of approximately 0.2 to 0.4, the surface albedo
84 drops to about 0.75 or even lower (0.15) as melt ponds grow and deepen (Singh and
85 Haritashya, 2011). These changes have been found to be important for the global energy
86 balance (Flanner et al., 2007; Hansen and Nazarenko, 2004) and, if enhanced by BC,
87 contribute to climate warming (Warren and Wiscombe, 1980).



88 Although BC in Arctic snow and ice has been found to be important for the Earth's
89 climate (Flanner et al., 2007; Sand et al., 2015), its large-scale temporal and spatial
90 distributions and exact origin are still poorly quantified (AMAP, 2015). Efforts to determine
91 the concentrations of BC in snow across the Arctic were made by Clarke and Noone (1985),
92 Doherty et al. (2010, 2013), (Forsström et al., 2013; Ingvander et al., 2013; McConnell et al.,
93 2007). This paper presents measurements of Elemental Carbon (EC) concentrations in snow
94 samples collected in spring 2014, 2015 and 2016 in the Kindo Peninsula (White Sea, Karelia),
95 around Arkhangelsk in northwestern European Russia, and in Western Siberia. In the latter
96 area, gas flaring emissions are very important. Flaring emissions are highly uncertain because
97 both activity data and emission factors are largely lacking. According to the Global Gas
98 Flaring Reduction Partnership (GGFR)
99 (<http://www.worldbank.org/en/programs/gasflaringreduction>), nearly 50 billion m³ of gas are
100 flared in Russia annually. The Russian flaring emissions in the Nenets/Komi regions and in
101 Khanty-Mansiysk are the major sources in the area. It has been reported that gas flaring in
102 Russia contributes about 42% to the annual average BC surface concentrations in the Arctic
103 (Stohl et al., 2013).

104 The use of the terms EC and BC has been the topic of several scientific papers (Andreae
105 and Gelencsér, 2006; Bond et al., 2013; Petzold et al., 2013). Petzold et al. (2013) defined BC
106 as a substance with 5 properties (see Table 1 in Petzold et al., 2013), for which no single
107 measurement instrument exists that is sensitive to all of them at the same time. Consequently,
108 BC cannot uniquely be measured, although some of its properties can, such as the absorption
109 coefficient σ_{ap} and the elemental carbon (EC) concentration, both commonly measured in
110 atmospheric monitoring networks across the world. Hence, the term BC should be used in a
111 qualitative manner. In the present study, EC measurement data from three campaigns are
112 compared to simulation results from the Lagrangian particle dispersion model (LPDM)
113 FLEXPART. The model is used here for the first time to quantify the sources contributing to
114 BC in snow in Russia adopting a special feature that was developed recently.

115 **2 Methodology**

116 **2.1 Collection and storage of snow samples**

117 Snow samples were collected along a north–south transect between Tomsk and the
118 Yamal coast in February–March 2014, while in March 2015 sample collection took place in
119 the Kindo Peninsula and near the port of Arkhangelsk near the White Sea (Figure 1). Finally,



120 in February–May 2016 samples were collected in the Kindo Peninsula, in Arkhangelsk and
121 between Tomsk and Yamal. These areas have been reported to receive pollution both from
122 urban pollution and gas flaring sources (Stohl et al., 2013). For example, the gas flaring
123 sources located in Yamal and Khanty-Mansiysk (Russia) are in the main pathway along
124 which sub-Arctic air masses travel to the Arctic (Stohl et al., 2006). All sampling points were
125 located more than 500 m away from roads to minimize the influence from local traffic
126 emissions. Information about the samples such as the location of sampling, the amount of
127 snow collected and the depth to which snow was sampled is reported in Table S1 and the
128 sample locations are plotted in Figure 1.

129 Sampling was performed using a metal-free technique, using pre-cleaned plastic shovels
130 and single-use vinyl gloves. Samples were stored in polyethylene bags, which had been
131 thoroughly washed with 1 M HCl and with abundant Milli-Q water in the laboratory prior to
132 their use. After returning the samples to the laboratory, the snow was allowed to melt at
133 ambient temperature (18–20°C), and immediately filtered through quartz fibre filters (47 mm
134 diameter 2500QAT-UP, Pall, for samples collected in 2014 and 47 mm diameter QM-A
135 Whatman for samples collected in 2015 and 2016). The filters were dried at 60–70°C,
136 wrapped in aluminum foil and stored in a refrigerator.

137 **2.2 Elemental Carbon measurements by Thermal–Optical Analysis (TOA)**

138 The filters' content of elemental carbon (EC) was measured at NILU's laboratories by
139 thermal-optical analysis (TOA), using the Sunset laboratory OC/EC instrument operated
140 according to the EUSAAR-2 protocol (Cavalli et al., 2010). A 1.5 cm² punch was cut from the
141 filtered snow samples for the analysis. Transmission was used for organic carbon (OC)
142 charring correction. The OC/EC instrument's performance is regularly intercompared as part
143 of the joint European Monitoring and Evaluation Programme (EMEP)/Aerosols, Clouds, and
144 Trace gases Research InfraStructure Network (ACTRIS) quality assurance and quality control
145 effort (Cavalli et al., 2015).

146 **2.3 Measurements of carbonate (CO₃²⁻)–carbon by Thermal–Optical Analysis** 147 **(TOA) following thermal-oxidative pre-treatment**

148 The content of carbonate (CO₃²⁻)–carbon on the filters was measured by TOA,
149 following thermal-oxidative pretreatment based on the approach described by Jankowski et al.
150 (2008). In brief, a punch of 1.5 cm² from each filter was heated at 450 °C for 2 hours in



151 ambient air to remove OC and EC, but not CO_3^{2-} -carbon. The filter punch was subjected to
152 TOA immediately (30 sec) after thermal-oxidative pre-treatment. The split time (between OC
153 and EC) obtained for each filter punch used to determine the filter samples' content of EC
154 (Chapter 2.2) was also used to apportion CO_3^{2-} -carbon to OC and/or EC. The influence of
155 CO_3^{2-} -carbon evolving as EC, was accounted for by the following equation:

$$EC_{CO_3^{2-}}^{corr} = EC - EC_{CO_3^{2-}}$$

156 where $EC_{CO_3^{2-}}^{corr}$ is elemental carbon corrected for CO_3^{2-} -carbon that evolves as EC during
157 TOA, EC is elemental carbon and $EC_{CO_3^{2-}}$ is CO_3^{2-} -carbon that evolves as EC during TOA.
158 EC values were 5-22% lower applying this correction (see Supplementary Information).

159 **2.4 Emissions and modelling of black carbon**

160 The concentrations of BC in snow were simulated with the LPDM FLEXPART version
161 10 (Stohl et al., 1998, 2005). The model was driven with 3-hourly (for the years 2014 and
162 2015) and hourly (for the year 2016) operational meteorological wind fields retrieved from
163 the European Centre for Medium-Range Weather Forecasts (ECMWF). The ECMWF data
164 have 137 vertical levels. The data used had a horizontal resolution of $1^\circ \times 1^\circ$ for the 2014 and
165 2015 simulations and $0.5^\circ \times 0.5^\circ$ for the 2016 ones.

166 The simulations were conducted in backwards time (“retroplume”) mode, using a new
167 feature of FLEXPART to reconstruct wet and dry deposition with backward simulations
168 (Eckhardt et al., 2017). This new feature is an extension of the traditional possibility to
169 simulate atmospheric concentrations backward in time (Seibert and Frank, 2004; Stohl et al.,
170 2003). It is computationally efficient because it requires only two single tracer transport
171 simulations (one for wet deposition, one for dry deposition) for each measurement sample. To
172 reconstruct wet deposition amounts of BC, computational particles were released at altitudes
173 of 0 to 20 km at the locations where snow samples were taken, whereas to reconstruct dry
174 deposition, particles were released between the surface and 30 m at these locations. All
175 released particles represent a unity deposition amount, which was converted immediately (i.e.,
176 upon release of a particle) to atmospheric concentrations using the deposition intensity as
177 characterized either by dry deposition velocity or scavenging rate (for further details, see
178 Eckhardt et al., 2017). The concentrations were subsequently treated as in normal
179 “concentration mode” backward tracking (Seibert and Frank, 2004) to establish source-
180 receptor relationships between the emissions and deposition amounts. The termination time of



181 the particle release was the time at which the snow sample was collected, whereas the
182 beginning time was set as the time when the ECMWF precipitation at the sampling site,
183 accumulated backward in time, was equal to the water equivalent of the snow sample, up to
184 the specified sampling depth.

185 The model output consists of a spatially gridded sensitivity of the BC deposition at the
186 sampling location (receptor) to the BC emissions, equivalent to the backwards time mode
187 output for concentrations (Seibert and Frank, 2004; Stohl et al., 2003). BC deposition at the
188 snow sampling point can be computed (in mass per area units) by multiplying the emission
189 sensitivity in the lowest model layer (the footprint emission sensitivity) with gridded
190 emissions from a BC emission inventory and integrating over the grid. The deposited BC can
191 be easily converted to BC snow concentration by taking into account the water equivalent
192 depth of the snow from ECMWF (in mm). In the present study, the ECLIPSE (Evaluating the
193 CLimate and Air Quality ImPacts of ShortlivEd Pollutants) version 5 emission inventory
194 (Klimont et al., 2016; Stohl et al., 2015) was used
195 (http://www.iiasa.ac.at/web/home/research/researchPrograms/air/Global_emissions.html).
196 The total emissions of BC from ECLIPSE in the areas of study are shown in Figure 1 (left
197 panel).

198 BC was assumed to have a density of 2 g m^{-3} in our simulations and a logarithmic size
199 distribution with an aerodynamic mean diameter of $0.25 \text{ }\mu\text{m}$ and a logarithmic standard
200 deviation of 0.3. Each computational particle released in FLEXPART represents an aerosol
201 population with a lognormal size distribution (see Stohl et al., 2005). Assumed aerodynamic
202 mean diameter and logarithmic standard deviation are used by FLEXPART's dry deposition
203 scheme, which is based on the resistance analogy (Slinn 1982), and they are consistent with
204 those used in other transport models (see Evangeliou et al., 2016; Shiraiwa et al., 2008).
205 Below-cloud scavenging was determined based on the precipitation rate taken from ECMWF.
206 The in-cloud scavenging was based on cloud liquid water and ice content, precipitation rate
207 and cloud depth from ECMWF (Grythe et al. 2016). The FLEXPART user manual (available
208 from <http://www.flexpart.eu>) provides more information. All modelling results for this
209 sampling campaign can be viewed interactively at the URL
210 http://niflheim.nilu.no/NikolaosPY/SnowBC_141516.py.

211 **3 Results**

212 **3.1 Elemental Carbon concentrations measured in snow**



213 The spatial distribution of EC measured in snow samples from northwestern European
214 Russia and Western Siberia is shown in Figure 1 for each of the campaigns (2014, 2015 and
215 2016). There was large spatial variability in the distribution of EC in snow in 2014 ranging
216 from 3 to 219 ng g⁻¹, with a median (\pm standard deviation) of 23 \pm 50 ng g⁻¹. The highest EC
217 concentrations in 2014 were observed in Western Siberia near Tomsk (147 to 219 ng g⁻¹).
218 FLEXPART emission sensitivities for these samples showed that the air was coming from the
219 north and the east (see in http://niflheim.nilu.no/NikolaosPY/SnowBC_141516.py). This
220 explains the high concentrations of EC, as most of the anthropogenic BC sources are located
221 in these regions. In the rest of the snow samples, EC concentrations between 4 and 170 ng g⁻¹
222 were observed. High concentrations were observed near the Ob River coinciding with air
223 masses arriving mainly from Europe. During the 2015 field campaign, EC concentrations
224 were the highest near Arkhangelsk (175 ng g⁻¹), for which FLEXPART showed that the air
225 was coming from nearby areas (http://niflheim.nilu.no/NikolaosPY/SnowBC_141516.py).
226 Therefore, it is likely that the samples were affected by direct emissions from the city or the
227 port of Arkhangelsk. During the same campaign, snow samples collected in the Kindo
228 peninsula (at the White Sea coast) showed high variability in EC concentrations (range: 46 –
229 152 ng g⁻¹, median=70 \pm 37 ng g⁻¹). According to FLEXPART emission sensitivities, air
230 masses were transported to Kindo peninsula from central and southern Europe driven by an
231 anticyclone over Scandinavia (http://niflheim.nilu.no/NikolaosPY/SnowBC_141516.py).
232 Finally, in 2016, snow samples were collected outside Arkhangelsk, at the Kindo peninsula,
233 as well as close to the Yamal Peninsula in Western Siberia (range: 7–161 ng g⁻¹, median:
234 40 \pm 39 ng g⁻¹). In Arkhangelsk, EC concentrations in snow varied widely in 2016 ranging
235 from 31 to 161 ng g⁻¹ with a median concentration in this region of 61 \pm 45 ng g⁻¹. This is far
236 below the 175 ng g⁻¹ observed in 2015, although there was only one sample collected in that
237 year. In the Kindo Peninsula, EC was relatively constant in 2016 ranging between 25 and 35
238 ng g⁻¹ (median = 28 \pm 4 ng g⁻¹), which is more than 60% lower compared with the 2015 values
239 (median = 70 \pm 37 ng g⁻¹). Finally, between Tomsk and Yamal EC was highly variable (7 – 119
240 ng g⁻¹) due to the different EC sources affecting snow (median = 50 \pm 38 ng g⁻¹). For instance,
241 it is expected that gas flaring affects snow close to Yamal, while snow collected in the south
242 (Tomsk) is likely influenced by sources in Europe or local urban emissions. Nevertheless, the
243 highest concentrations (>100 ng g⁻¹) were observed north of 68°N, in the Yamal Peninsula.

244 We compared the measured snow concentrations with those calculated by FLEXPART.
245 For this, the emission sensitivities were multiplied with the total emission fluxes from



246 ECLIPSE (section 2.4). A scatter plot is presented in Figure 1 (middle panel). The results
247 show good quantitative agreement and a good correlation between modelled BC and
248 measured EC concentrations for the 2015 and 2016 campaigns ($R_{2015} = 0.83$ and $R_{2016} =$
249 0.68 , $p - value < 0.05$), but weaker correlation for 2014 ($R_{2014} = 0.53$, $p - value <$
250 0.05). For further validation, the fractional bias (FB) of each individual sample was calculated
251 together with the mean fractional bias (MFB) for observed EC and modelled BC for the 2014,
252 2015 and 2016 sampling campaigns as follows:

$$FB = \frac{C_m - C_o}{(C_m + C_o)/2} \times 100\% \text{ and } MFB = \frac{1}{N} \sum_{i=1}^N \frac{C_m - C_o}{(C_m + C_o)/2} \times 100\%$$

253 where C_m and C_o are the modelled BC and measured EC concentrations and N is the total
254 number of observations for each year. The FB for individual samples is shown in Figure S 1.
255 FB is a useful model performance indicator because it is symmetric and gives equal weight to
256 underestimations and overestimations (it takes values between -200% and 200%). It is used
257 here to show the locations where modelled BC concentrations in snow over- or underestimate
258 observations (see Figure S 1). The MFB of the model for the 2014 snow measurements was -
259 42%. In total, the model underestimated concentrations for 17 out of 23 samples with FB
260 values ranging from -168% to -30%, whereas for the rest (six samples) FB values ranged
261 between 20% and 148% (median: $-56\% \pm 81\%$) (Figure S 1). In 2015, the MFB of the model
262 was -48% (median: $-56\% \pm 32\%$), where 11 out of 12 values were underestimated by the model
263 showing FB values that ranged between -101% and -7% (one FB value was found to be 12%).
264 Finally, FB values of the simulated concentrations of BC in snow showed another
265 underestimation for 2016 (median: $-13\% \pm 73\%$) varying from -198% to -0.3% for 12 out of
266 19, whereas for seven samples the model predicted higher concentrations compared with
267 observations (10% to 75%) (Figure S 1). Furthermore, the root mean square error (RMSE)
268 was computed, which is a frequently used measure of the differences between values
269 predicted by a model and the values actually observed. RMSE values were estimated to be
270 quite high, between 37 and 49 ng g^{-1} , due to the large variation of the observed EC
271 concentrations.

272 The levels of EC in snow presented here are relatively high compared to previously
273 reported concentrations in the Arctic. Excluding Aamaas et al. (2011) who reported EC
274 concentration in snow close to the Svalbard airport greater than 1000 ng g^{-1} , Ruppel et al.
275 (2014) found that EC concentrations have been increasing up to 103 ng g^{-1} since 1970 in



276 Svalbard. McConnell et al. (2007) reported that the BC concentrations measured at the D4
277 ice-core site in Greenland were 10 ng g^{-1} , at maximum, which most likely originated from
278 biomass burning in the conifer-rich boreal forest of the Eastern and Northern United States
279 and Canada. Forsström et al. (2013) reported concentrations as high as 88 ng g^{-1} in
280 Scandinavia, and lower ones at higher latitudes ($11\text{--}14 \text{ ng g}^{-1}$ in Svalbard, $7\text{--}42 \text{ ng g}^{-1}$ in the
281 Fram Strait, and 9 ng g^{-1} in Barrow). Svensson et al. (2013) collected snow samples from
282 Tyresta National Park and Pallas-Yllästunturi National Park in Sweden. Tyresta is a relatively
283 polluted site located circa 25 km from the city centre of Stockholm (population of about 2
284 million people). Yllästunturi National Park is located in Arctic Finland and a clean site with
285 no major city influencing the local and regional air. The concentration of EC in Pallas-
286 Yllästunturi was between 0 and 140 ng g^{-1} , while in Tyresta the BC concentrations were one
287 order of magnitude higher ($53\text{--}810 \text{ ng g}^{-1}$). Furthermore, Doherty et al. (2010) in the most
288 complete dataset for the Arctic snow and ice BC reported highly variable concentrations (up
289 to 800 ng g^{-1}) for five consecutive years (2005–2009). Finally, in the most recent dataset for
290 snow BC (Macdonald et al., 2017), concentrations ranging from 0.3 to 15 ng g^{-1} were reported
291 for samples collected near the Alert observatory (see section 4.1).

292 3.2 Sources and origin of BC

293 We further analysed the model output in order to calculate relevant contributions from
294 various BC source types to BC concentrations in snow (for method description, see section
295 2.4). ECLIPSE emissions account for waste burning (WST), industrial combustion and
296 processing (IND), surface transportation (TRA), power plants, energy conversion, and
297 extraction (ENE), residential and commercial combustion (DOM), gas flaring (FLR), whereas
298 biomass burning (BB) emissions were adopted from the Global Fire Emissions Database,
299 Version 4 (GFEDv4.1) (Giglio et al., 2013). The results are depicted in Figure 2 for the
300 sampling campaigns of 2014, 2015 and 2016 in Western Siberia and North-Western European
301 Russia, sorted from the northernmost to the southernmost sampling location.

302 In 2014, TRA contributed about 18%, on average, to the simulated BC in snow, DOM
303 28%, FLR 44%, whereas ENE and IND were less significant. Maxima of TRA, DOM, and
304 FLR contributions were observed at a latitude of about 65°N , where measured EC and
305 modelled BC were similar. An example of the contribution from the aforementioned
306 dominant sources to snow BC concentrations for the highest measured EC concentration in
307 snow is shown in Figure 3. The transport sector includes emissions from all land-based



308 transport of goods, animals and persons. It is more significant in southern Russia and close to
309 the borders with Kazakhstan and Mongolia, where a large number of major Russian cities are
310 located (e.g., Moscow, Kazan, Voronezh, Saratov, Samara, Ufa, Perm, Yekaterinburg,
311 Tyumen, Omsk, Tomsk, Novosibirsk, Krasnoyarsk, etc...) and connected with each other by
312 federal highways. Residential and commercial combustion includes emissions from
313 combustion in households and public and commercial buildings. Therefore, it is important for
314 areas with large population centres (Figure 3). FLR emissions were found to contribute the
315 most in this example with a total concentration from this sector of 19.7 ng g^{-1} (relative to 12.6
316 and 16.5 ng g^{-1} in TRA and DOM, respectively) (Figure 3).

317 In the Kindo Peninsula and in Arkhangelsk, where snow sampling took place in 2015,
318 the main contributions to snow BC were from DOM (47%), TRA (30%), BB (7%), and FLR
319 (6%) (Figure 2). Similar to EC measurements in snow, simulated BC was also higher than in
320 2014, as the sampling sites were located closer to strong sources in Europe (Kindo) and close
321 to a populated area (Arkhangelsk) with a strong regional impact. The highest concentration of
322 EC was observed in the Kindo Peninsula ($33.13^{\circ}\text{E} - 66.53^{\circ}\text{N}$). Figure 4 shows the spatial
323 distribution of emissions that contributed to simulated snow BC at the sampling point where
324 the highest BC concentration was observed. In this case, TRA and DOM emissions from
325 Europe mostly affected snow in the Kindo Peninsula, whereas FLR emissions were very low
326 due to the large distance from the sampling point. Emissions from an unusual late winter/early
327 spring episode of BB in the borders of Belarus, Ukraine and Russia also affected snow
328 concentrations in northwestern European Russia (Figure 4). The importance of episodic BB
329 releases in Russia and the miscalculation of satellite retrieved BB emissions and their impact
330 in Arctic concentrations in early spring has been explained by Evangeliou et al. (2016) and
331 Hao et al. (2016). BB emissions contributed about 19.4 ng g^{-1} to the snow concentration at the
332 receptor point, mostly originating from Eastern Europe (Figure 4). TRA and DOM emissions
333 were the dominant sources for this sampling point, contributing 33.6 and 47.2 ng g^{-1} ,
334 respectively (Figure 4).

335 Finally, in 2016, when samples were collected at the Kindo Peninsula, in Arkhangelsk
336 and in Yamal, DOM contributed 31%, FLR about 29% and TRA 27%, on average (Figure 2,
337 bottom). Similar to the measured EC concentrations in snow, simulated concentrations of BC
338 in 2016 were lower than those in 2015, on average. The highest measured EC concentration
339 was observed in the Khanty-Mansiysk region ($72.94^{\circ}\text{E} - 65.36^{\circ}\text{N}$), which mirrors the
340 simulated BC concentration at the same point very well. The much higher contribution from



341 TRA at this sampling point (38.6 ng g^{-1}) (Figure 5) is attributed to emissions from Southern
342 Russia (e.g., Tomsk), where all the main cities in Russia are located. Another large fraction of
343 TRA emissions comes from Central and Eastern Europe (see also in
344 http://niflheim.nilu.no/NikolaosPY/SnowBC_141516.py). Similar to TRA, emissions from
345 DOM were mostly transported to Khanty-Masiysk from Central and Eastern Europe, as well
346 as from Turkey contributing 36.6 ng g^{-1} (Figure 5). As previously mentioned, the sampling
347 point where the highest EC concentration was measured is located inside the largest gas
348 flaring region of Russia. In addition, the corresponding emission sensitivity maps showed that
349 the air was coming from south passing directly through this high emission region making FLR
350 emissions the highest contributing source (88.8 ng g^{-1}) (Figure 5).

351 4 Discussion

352 4.1 Cross validation of modelled BC concentrations with public datasets

353 In this section, we present an effort to further validate our model calculations of BC
354 concentrations in snow. For this purpose, BC concentrations in snow were adopted from
355 Doherty et al. (2010) and FLEXPART BC concentrations were simulated as described in
356 section 2.4. Samples were collected in Alaska, Canada, Greenland, Svalbard, Norway, Russia,
357 and the Arctic Ocean during 2005–2009, on tundra, glaciers, ice caps, sea ice, frozen lakes,
358 and in boreal forests. Snow was collected mostly in spring, when the combination of snow
359 cover and exposure to sunlight is at maximum and before the snow had started to melt.
360 Samples of melting snow collected in the summer of 2008 from Greenland and from Tromsø,
361 Norway, were removed from the study, as we have no knowledge about the depth of the melt
362 layer and effects of the percolation of meltwater through the snowpack. All samples were
363 collected away from local sources of pollution. In many locations (Canadian Arctic, Russia,
364 Greenland, Tromsø and Ny-Ålesund) samples were gathered at different depths throughout
365 the snowpack, giving information on the seasonal evolution of BC concentrations as the snow
366 accumulated (and/or sublimated) throughout the winter. In these cases only the surface BC
367 was taken into account. The snow was melted and filtered, and the filters were analysed in a
368 specially designed spectrophotometer system to infer the concentration of BC (for more
369 information see Doherty et al., 2010).

370 A comparison of measured and modelled BC concentrations in snow is depicted in
371 Figure S 2. The model captures snow BC concentrations effectively in most of the Arctic
372 regions except for the Canadian Arctic, where the modelled concentrations of snow in 2007



373 were significantly higher. Samples from the same region in other years showed good
374 agreement with modelled values. The model generally tends to underestimate deposition with
375 a MFB of -51%, similar to our finding for the new Russian measurements. The RMSE was
376 estimated to be 52 ng g^{-1} , which is acceptable considering that the variation of snow
377 concentrations in the dataset ranged from 0.3 to 783 ng g^{-1} . The highest measured
378 concentrations of snow BC were observed in Russia, where the model showed a good spatial
379 agreement. For instance, the highest values were obtained in Western Siberia, close to the gas
380 flaring regions of the Nenets/Komi oblast, as well as in southeastern and northeastern Russia,
381 where air masses were arriving from high emitting sources in southeastern Asia. Lower biases
382 in modelled BC concentrations were observed in northern Siberia with the exception of a few
383 samples at the coasts of the Kara Sea and northeastern Siberia. Furthermore, biased BC
384 concentrations were also observed in Greenland and northern Canada. In Western Siberia, BC
385 in snow presented in Doherty et al. (2010) between 2005–2009 was $101 \pm 153 \text{ ng g}^{-1}$ on
386 average, which is very close to the average value of measured EC obtained from the sampling
387 2014–2016 campaigns ($83 \pm 37 \text{ ng g}^{-1}$).

388 Moreover, our model was also compared with snow samples collected in a recent
389 campaign presented in Macdonald et al. (2016). These snow samples were collected at the
390 Global Atmosphere Watch Observatory at Alert, Nunavut, from September 14th, 2014 to June
391 1st, 2015. Alert is a remote outpost in the Canadian high Arctic, at the northern coast of
392 Ellesmere Island ($82^{\circ}27' \text{ N}$, $62^{\circ}30' \text{ W}$), with a small transient population of research and
393 military personnel. Sampling details and analytical methodologies used for the analysis of BC
394 can be found in Macdonald et al. (2016). BC concentrations in FLEXPART were simulated as
395 in all previous analyses described in this paper (see section 2.4.). Timeseries of simulated and
396 measured BC are depicted in Figure S 3 for the whole sampling period. As before, the quite
397 high correlation coefficient (R) of 0.63 indicates that our model captures the temporal
398 variation of the measured BC in snow. The RMSE was estimated to be almost 63 ng g^{-1} , a
399 relatively high value. The MFB of 47% indicates a strong overestimation of snow
400 concentrations, although in many samples the opposite was also observed (Figure S 3). This is
401 in contrast to the previous data sets discussed, for which the model underestimated.

402 We have further tried to further analyse the origin of the aforementioned
403 overestimations in the Canadian Arctic in both datasets (Doherty et al., 2010; Macdonald et
404 al., 2017), as they are shown to be rather systematic. For this reason, we have calculated the
405 average footprint emission sensitivities and the average BC contribution from the major



406 sources in ECLIPSE for the 2007 snow samples in the Canada Arctic and for Alert samples
407 that were three or more times higher than the observations, in order to locate the simulated
408 overestimations (Figure 6).

409 Regarding the model overestimation for the 2007 samples, the average footprint
410 emission sensitivity showed that the air was coming from continental regions of Canada with
411 a smaller contribution from Scandinavia (Figure 6). The highest emission sources for these
412 samples were TRA and DOM that contributed almost 80% to the snow concentrations,
413 whereas forest fires were less important at the time of sampling. Two hot spot areas were
414 identified, one along the borders of Canada with USA and another in southeastern Asia of
415 smaller intensity. A similar emission sensitivity was obtained for the same area of the
416 Canadian Arctic in 2009 only slightly shifted to the north, whereas modelled concentrations
417 were in very good agreement with observations (Figure S 2). This shows that the model
418 overestimation for the 2007 samples is likely attributed to an overestimation of TRA and
419 DOM sources in North America in ECLIPSE for 2007. For the Alert samples that the model
420 strongly overestimated BC, the major sources were TRA and FLR, which contributed 55%,
421 and BB which contributed about 7 ng g^{-1} on average (Figure 6). Anthropogenic BC arriving
422 from Europe and Russia has been previously shown to be important for Alert air
423 concentrations (Sharma et al., 2013). The model overestimation of BC in snow samples at
424 Alert needs further investigation. It is likely that it originates from anthropogenic emissions in
425 northwestern America or in Europe, because forest fires in Canada and Russia, although
426 important for Alert (e.g., Qi et al., 2017), were not significant in the present comparison.

427 **4.2 Model deviation from snow EC measurements and region-specific** 428 **contribution of sources**

429 It was already shown that, on average, measured concentrations of EC in snow in
430 northwestern European Russia and Western Siberia were underestimated in FLEXPART
431 (Figure 2). This was confirmed by the calculated fractional bias (see section 3.2), the spatial
432 distribution of which is shown already in Figure S 1. To examine whether this
433 underestimation was due to missing emission sources or errors in modelled transport and
434 deposition, we have calculated the average footprint emission sensitivity for those sampling
435 points, for which FLEXPART strongly ($FB < -100\%$) and slightly ($-100\% < FB < 0\%$)
436 underestimated the observed values. The average footprint emission sensitivities are shown in
437 Figure 7 together with the locations of the active fires of the last two months until collection



438 of snow samples adopted from MODIS (Moderate Resolution Imaging Spectroradiometer)
439 (Giglio et al., 2003) and the gas flaring facilities from the Global Gas Flaring Reduction
440 Partnership (GGFR) (<http://www.worldbank.org/en/programs/gasflaringreduction>).

441 When the model strongly underestimated the measured EC ($FB < -100\%$), the
442 average footprint emission sensitivity showed the highest values over the Yamal Peninsula
443 and the agglomeration of many gas flares in Khanty-Mansiysk (Figure 7). This might confirm
444 the finding of Huang et al. (2014) that gas flaring emissions in the ECLIPSE inventory, while
445 very high, are still underestimated. According to a related study, Russia contributes 57% to
446 the global BC emissions from gas flaring (Huang and Fu, 2016). Underestimation of modelled
447 atmospheric concentrations compared to observations from the Barents and Kara Seas was
448 recently also reported by Popovicheva et al. (2017), although the underestimation was
449 relatively small.

450 When the model showed a moderate underestimation of EC concentrations in snow
451 ($-100\% < FB < 0\%$), the emission sensitivity was high near Arkhangelsk and over
452 Scandinavia (Figure 7). BC emissions in Scandinavia are considered relatively low in most
453 inventories and contribute no more than 6.5% to the global emissions in ACCMIP (Aerosol
454 Chemistry Climate Model Intercomparison Project) (Lamarque et al., 2013), 6.2% in
455 EDGARv4.2 (Emission Database for Global Atmospheric Research) (Olivier et al., 2005),
456 2.1% in MACCity (Monitoring Atmospheric Composition & Climate / megaCITY - Zoom for
457 the ENvironment) (Hollingsworth et al., 2008; Stein et al., 2012) and 3.3% in ECLIPSE
458 (Klimont et al., 2016). The highest emission sensitivity was found over northwestern Russia
459 though (Figure 7), where Murmansk is located. Pollution in Murmansk can be high due to
460 emissions from local industry, mining, heating and transport (Law and Stohl, 2007). Another
461 potential source region was Nenets/Komi area and Western Kazakhstan, where a few other
462 flaring facilities are located (Figure 7).

463 Figure 7 shows that the underestimation of observed EC concentrations in snow
464 strongly depends on the region, where samples are collected. In Western Siberia, the
465 underestimation was larger than in northwestern European Russia. For this reason, we have
466 computed the average region-specific emission sensitivities and the average region-specific
467 contribution from the major polluting sources of ECLIPSE. We distinguish between three
468 regions, northwestern European Russia, Western Siberia (north of 62 °N) and Western Siberia
469 (south of 62 °N) (Figure S 4 – S 6). For the samples collected in northwestern European



470 Russia (Figure S 4), an average contribution of 21.6 ng g^{-1} from all sources was estimated
471 mainly originating mainly from TRA (7.7 ng g^{-1}) and DOM (10.4 ng g^{-1}) sources in Finland.
472 The contribution from BB and FLR emissions was insignificant, whereas the rest of the
473 ECLIPSE sources were negligible (IND, ENE, WST). For the samples collected at high
474 latitudes in Western Siberia (Figure S 5), the average contribution from all sources was more
475 than 4 times higher (86 ng g^{-1}) than those observed in northwestern European Russia. FLR
476 emissions accounted for 40% of the total reflecting the proximity to the main flaring facilities
477 of Russia. Another 24% of the average contribution was attributed to TRA activities in
478 Europe and southeastern Russia that affect the northern part of Western Siberia, although they
479 are rather remote. Finally, DOM emissions in Eastern Europe also contributed another 28%.
480 Finally, for the samples that were collected in the southern part of the Western Siberia (Figure
481 S 6) an average contribution of 47.4 ng g^{-1} was estimated from all sources included in
482 ECLIPSE. Again, the highest contributing sub-categories were TRA and DOM, whereas FLR
483 appeared to contribute rather insignificantly considering that the sampling area is close to
484 Khanty-Mansiysk flaring region.

485 Overall, the region-specific analysis of the sources contributing to modelled BC in
486 snow showed that the DOM, FLR and/or TRA sources might explain the model
487 underestimation in high Arctic. However, in the most recent assessments of BC of the higher
488 Arctic (Popovicheva et al., 2017; Winiger et al., 2017), it was shown that ECLIPSE captures
489 levels of BC quite well, whereas FLR emissions might have a smaller impact in the Central
490 Siberian Arctic (Tiksi) than previously estimated. Surprisingly, the average contribution from
491 BB in lower latitudes was extremely low in all Western Siberia (Figure S 5 and S 6), despite
492 the fact that sampling took place in springtime, where BB becomes important. Evangeliou et
493 al. (2016) reported that using a different dataset, that is based on the same approach as GFED,
494 but includes updated emission factors for Eurasia, surface concentrations of BC in the Arctic
495 stations can be substantially higher. This shows the need for further investigation of BC
496 sources in the Russian Arctic.

497 5 Conclusions

498 We have analysed snow samples collected in Western Siberia and northwestern
499 European Russia during 2014, 2015 and 2016 with respect to EC. This region is of major
500 interest due to its large uncertainty in BC emissions and because it is located in the main



501 transport route of BC to the Arctic. An effort to constrain the sources that contribute to the
502 measured concentrations of BC in snow was made using the LPDM FLEXPART (version 10).

503 The observed EC levels in snow varied widely within and between regions (3–219 ng g⁻¹
504 ¹ for 2014, 46–175 ng g⁻¹ in 2015 and 7–161 ng g⁻¹ in 2016), and are in the upper range of
505 previously reported concentrations of EC and BC in snow in the Arctic region. However, the
506 observed levels presented here appear typical for Western Siberia, which is subject to high
507 domestic Russian emissions, as well as to transport from distant European ones.

508 The snow BC concentrations predicted by the model are in good agreement with EC
509 observations over Western Siberia and northwestern European Russia ($R = 0.5 - 0.8$).
510 However, the calculated MFB values (-48% to -27%) showed that the model systematically
511 underestimated observations in Russia. This underestimation strongly depended on the region
512 where the samples were collected. In northwestern European Russia, the main contributing
513 sources were TRA and DOM mainly from adjacent regions in Finland. TRA and DOM
514 contributed double to snow BC sampled at low latitudes of Western Siberia (<60°N), with the
515 majority of the emissions to originate from highly populated centres in Central Europe.
516 Finally, in higher latitudes of Western Siberia (>60°N), snow BC concentrations were further
517 increased mainly due to FLR emissions from facilities located close to the snow sampling
518 points.

519 The modelled BC concentrations in snow were further investigated using two
520 independent public measurement datasets that include samples from all over the Arctic for the
521 period 2005 to 2009 and from Alert in 2014 and 2015. The model captured levels of BC quite
522 effectively despite the large variation in measured concentrations. An exception was observed
523 in North America in spring 2007 and in Alert observatory in late winter – early spring 2015.
524 In both cases, the major sources were along the Canadian borders with USA and in Western
525 Europe. Considering that similar deviations were not observed in the area in samples collected
526 during other years, it is likely that some of the prevailing sources of BC there show strong
527 temporal variability in their emissions, and this is not taken into account in ECLIPSE.
528 Overall, previously reported measurements of snow BC in Western Siberia and northwestern
529 European Russia were 101 ± 153 ng g⁻¹ on average, which is about 20% higher than the EC
530 measurements presented here (83 ± 37 ng g⁻¹).

531 **Data availability.** All data used for the present publication can be obtained from the
532 corresponding author upon request.



533 *Competing interests.* The authors declare that they have no conflict of interest.

534 *Acknowledgements.* We would like to acknowledge the project entitled “Emissions of
535 Short-Lived Climate Forcers near and in the Arctic (SLICFONIA)”, which was funded by the
536 NORRUSS research program of the Research Council of Norway (Project ID: 233642) and
537 the Russian Fund for Basic Research (project No. 15-05-08374) for funding snow sampling in
538 the White Sea catchment area. We also thank Sergey Belorukov, Andrey Boev, Anton
539 Bulokhov, Victor Drozdov, Sergey Kirpotin, Ivan Kritzkov, Rinat Manasypov, Ivan
540 Semenyuk, and Alexander Yakovlev for helping during the three expeditions and
541 Academician Alexander P. Lisitzin for his valuable recommendations. O. S. Pokrovsky and S.
542 N. Vorobiev acknowledge support from BIO-GEO-CLIM grant No 14.B25.31.0001 for
543 sampling in Western Siberia. Acknowledgements are also owed to IIASA (especially Chris
544 Heyes and Zig Klimont) for providing the BC emission dataset. Computational and storage
545 resources for the FLEXPART simulations have been provided by NOTUR (NN9419K) and
546 NORSTORE (NS9419K). All plots from FLEXPART simulations have been included in an
547 interactive website for fast visualization
548 (http://niflheim.nilu.no/NikolaosPY/SnowBC_141516.py). All results can be accessed upon
549 request to the corresponding author of this manuscript.

550 *Author Contributions.* N. Evangeliou designed and performed the modelling experiments
551 and wrote the paper. V. P. Shevchenko organised and performed the sampling of EC, K.-E.
552 Yttri performed all the TOA of the snow samples. S. Eckhardt modified FLEXPART model
553 for the calculation of footprint emission sensitivities for deposited mass. E. Sollum wrote an
554 algorithm that computes the starting date of the FLEXPART releases based on the water
555 equivalent volume from ECMWF. O. S. Pokrovsky, V. O. Kobelev, V. B. Korobov, A. A.
556 Lobanov, D. P. Starodymova and S. N. Vorobiev assisted the sampling campaigns in Western
557 Siberia and northwestern European Russia during 2014–2016. R. L. Thompson and A. Stohl
558 supervised the study and wrote parts of the paper.

559

560 **References**

561 Aamaas, B., Bøggild, C. E., Stordal, F., Berntsen, T., Holmén, K. and Ström, J.: Elemental
562 carbon deposition to Svalbard snow from Norwegian settlements and long-range transport,
563 Tellus, Ser. B Chem. Phys. Meteorol., 63(3), 340–351, doi:10.1111/j.1600-
564 0889.2011.00531.x, 2011.



- 565 AMAP: AMAP assessment 2015: Black carbon and ozone as Arctic climate forcers, Arctic
566 Monitoring and Assessment Programme (AMAP), Oslo, Norway., 2015.
- 567 Andreae, M. O. and Gelencsér, A.: Black carbon or brown carbon? The nature of light-
568 absorbing carbonaceous aerosols, *Atmos. Chem. Phys.*, 6(3), 3419–3463, doi:10.5194/acpd-6-
569 3419-2006, 2006.
- 570 Bond, T. C., Streets, D. G., Yarber, K. F., Nelson, S. M., Woo, J. H. and Klimont, Z.: A
571 technology-based global inventory of black and organic carbon emissions from combustion, *J.*
572 *Geophys. Res. D Atmos.*, 109(14), 1–43, doi:10.1029/2003JD003697, 2004.
- 573 Bond, T. C., Doherty, S. J., Fahey, D. W., Forster, P. M., Berntsen, T., Deangelo, B. J.,
574 Flanner, M. G., Ghan, S., Kärcher, B., Koch, D., Kinne, S., Kondo, Y., Quinn, P. K., Sarofim,
575 M. C., Schultz, M. G., Schulz, M., Venkataraman, C., Zhang, H., Zhang, S., Bellouin, N.,
576 Guttikunda, S. K., Hopke, P. K., Jacobson, M. Z., Kaiser, J. W., Klimont, Z., Lohmann, U.,
577 Schwarz, J. P., Shindell, D., Storelvmo, T., Warren, S. G. and Zender, C. S.: Bounding the
578 role of black carbon in the climate system: A scientific assessment, *J. Geophys. Res. Atmos.*,
579 118(11), 5380–5552, doi:10.1002/jgrd.50171, 2013.
- 580 Brandt, R. E., Warren, S. G., Worby, A. P. and Grenfell, T. C.: Surface albedo of the
581 Antarctic sea ice zone, *J. Clim.*, 18(17), 3606–3622, doi:10.1175/JCLI3489.1, 2005.
- 582 Cavalli, F., Viana, M., Yttri, K. E., Genberg, J. and Putaud, J.-P.: Toward a standardised
583 thermal-optical protocol for measuring atmospheric organic and elemental carbon: the
584 EUSAAR protocol, *Atmos. Meas. Tech.*, 3(1), 79–89, doi:doi:10.5194/amt-3-79-2010, 2010.
- 585 Cavalli, F., Putaud, J.-P. and Yttri, K. E.: Availability and quality of the EC and OC
586 measurements within EMEP, including results of the fifth interlaboratory comparison of
587 analytical methods for carbonaceous particulate matter within EMEP (2012)., 2015.
- 588 Clarke, A. D. and Noone, K. J.: Soot in the arctic snowpack: a cause for perturbations in
589 radiative transfer, *Atmos. Environ.*, 41(SUPPL.), 64–72, doi:10.1016/0004-6981(85)90113-1,
590 1985.
- 591 Doherty, S. J., Warren, S. G., Grenfell, T. C., Clarke, A. D. and Brandt, R. E.: Light-
592 absorbing impurities in Arctic snow, *Atmos. Chem. Phys.*, 10(23), 11647–11680,
593 doi:10.5194/acp-10-11647-2010, 2010.



- 594 Doherty, S. J., Grenfell, T. C., Forsström, S., Hegg, D. L., Brandt, R. E. and Warren, S. G.:
595 Observed vertical redistribution of black carbon and other insoluble light-absorbing particles
596 in melting snow, *J. Geophys. Res. Atmos.*, 118(11), 5553–5569, doi:10.1002/jgrd.50235,
597 2013.
- 598 Eckhardt, S., Cassiani, M., Evangeliou, N., Sollum, E., Pisso, I. and Stohl, A.: Source-
599 receptor matrix calculation for deposited mass with the Lagrangian particle dispersion model
600 FLEXPART v10.2 in backward mode, *Geosci. Model Dev. Discuss.*, submitted, 2017.
- 601 Evangeliou, N., Balkanski, Y., Hao, W. M., Petkov, A., Silverstein, R. P., Corley, R.,
602 Nordgren, B. L., Urbanski, S. P., Eckhardt, S., Stohl, A., Tunved, P., Crepinsek, S., Jefferson,
603 A., Sharma, S., Nøjgaard, J. K. and Skov, H.: Wildfires in northern Eurasia affect the budget
604 of black carbon in the Arctic—a 12-year retrospective synopsis (2002–2013), *Atmos. Chem.*
605 *Phys.*, 16(12), 7587–7604, doi:10.5194/acp-16-7587-2016, 2016.
- 606 Flanner, M. G., Zender, C. S., Randerson, J. T. and Rasch, P. J.: Present-day climate forcing
607 and response from black carbon in snow, *J. Geophys. Res. Atmos.*, 112(11), 1–17,
608 doi:10.1029/2006JD008003, 2007.
- 609 Forsström, S., Isaksson, E., Skeie, R. B., Ström, J., Pedersen, C. A., Hudson, S. R., Berntsen,
610 T. K., Lihavainen, H., Godtliebsen, F. and Gerland, S.: Elemental carbon measurements in
611 European Arctic snow packs, *J. Geophys. Res. Atmos.*, 118(24), 13614–13627,
612 doi:10.1002/2013JD019886, 2013.
- 613 Forster, C., Wandinger, U., Wotawa, G., James, P., Mattis, I., Althausen, D., Simmonds, P.,
614 O’Doherty, S., Jennings, S. G., Kleefeld, C., Schneider, J., Trickl, T., Kreipl, S., Jäger, H. and
615 Stohl, A.: Transport of boreal forest fire emissions from Canada to Europe, *J. Geophys. Res.*,
616 106, 22887, doi:10.1029/2001JD900115, 2001.
- 617 Giglio, L., Descloitres, J., Justice, C. O. and Kaufman, Y. J.: An enhanced contextual fire
618 detection algorithm for MODIS, *Remote Sens. Environ.*, 87(2–3), 273–282,
619 doi:10.1016/S0034-4257(03)00184-6, 2003.
- 620 Giglio, L., Randerson, J. T. and van der Werf, G. R.: Analysis of daily, monthly, and annual
621 burned area using the fourth-generation global fire emissions database (GFED4), *J. Geophys.*
622 *Res. Biogeosciences*, 118, 317–328, doi:10.1002/jgrg.20042, 2013, 2013.
- 623 Grythe, H., Kristiansen, N. I., Groot Zwaafink, C. D., Eckhardt, S., Ström, J., Tunved, P.,



- 624 Krejci, R. and Stohl, A.: A new aerosol wet removal scheme for the Lagrangian particle
625 model FLEXPARTv10, *Geosci. Model Dev.*, 10, 1447–1466, doi:10.5194/gmd-10-1447-
626 2017, 2017.
- 627 Hansen, J. and Nazarenko, L.: Soot climate forcing via snow and ice albedos, *Proc. Natl.*
628 *Acad. Sci. U. S. A.*, 101(2), 423–428, doi:10.1073/pnas.2237157100, 2004.
- 629 Hao, W. M., Petkov, A., Nordgren, B. L., Silverstein, R. P., Corley, R. E., Urbanski, S. P.,
630 Evangeliou, N., Balkanski, Y. and Kinder, B.: Daily black carbon emissions from fires in
631 Northern Eurasia from 2002 to 2013, *Geosci. Model Dev. Discuss.*, (April), 1–24,
632 doi:10.5194/gmd-2016-89, 2016.
- 633 Hegg, D. A., Warren, S. G., Grenfell, T. C., Doherty, S. J., Larson, T. V. and Clarke, A. D.:
634 Source attribution of black carbon in arctic snow, *Environ. Sci. Technol.*, 43(11), 4016–4021,
635 doi:10.1021/es803623f, 2009.
- 636 Hollingsworth, A., Engelen, R. J., Textor, C., Benedetti, A., Boucher, O., Chevallier, F.,
637 Dethof, A., Elbern, H., Eskes, H., Flemming, J., Granier, C., Kaiser, J. W., Morcrette, J. J.,
638 Rayner, P., Peuch, V. H., Rouil, L., Schultz, M. G. and Simmons, A. J.: Toward a monitoring
639 and forecasting system for atmospheric composition: The GEMS project, *Bull. Am. Meteorol.*
640 *Soc.*, 89(8), 1147–1164, doi:10.1175/2008BAMS2355.1, 2008.
- 641 Huang, K. and Fu, J. S.: Data Descriptor : A global gas fl aring black carbon emission rate
642 dataset from 1994 to 2012, *Nature*, 1–11, doi:10.1038/sdata.2016.104, 2016.
- 643 Huang, K., Fu, J. S., Hodson, E. L., Dong, X., Cresko, J., Prikhodko, V. Y., Storey, J. M. and
644 Cheng, M. D.: Identification of missing anthropogenic emission sources in Russia:
645 Implication for modeling arctic haze, *Aerosol Air Qual. Res.*, 14(7), 1799–1811,
646 doi:10.4209/aaqr.2014.08.0165, 2014.
- 647 Ingvander, S., Rosqvist, G., Svensson, J. and Dahlke, H. E.: Seasonal and interannual
648 variability of elemental carbon in the snowpack of Storglaci??ren, northern Sweden, *Ann.*
649 *Glaciol.*, 54(62), 50–58, doi:10.3189/2013AoG62A229, 2013.
- 650 Jankowski, N., Schmidl, C., Marr, I. L., Bauer, H. and Puxbaum, H.: Comparison of methods
651 for the quantification of carbonate carbon in atmospheric PM10 aerosol samples, *Atmos.*
652 *Environ.*, 42(34), 8055–8064, doi:10.1016/j.atmosenv.2008.06.012, 2008.



- 653 Klimont, Z., Kupiainen, K., Heyes, C., Purohit, P., Cofala, J., Rafaj, P., Borken-Kleefeld, J.
654 and Schöpp, W.: Global anthropogenic emissions of particulate matter including black
655 carbon, *Atmos. Chem. Phys. Discuss.*, (October), 1–72, doi:10.5194/acp-2016-880, 2016.
- 656 Lamarque, J. F., Shindell, D. T., Josse, B., Young, P. J., Cionni, I., Eyring, V., Bergmann, D.,
657 Cameron-Smith, P., Collins, W. J., Doherty, R., Dalsoren, S., Faluvegi, G., Folberth, G.,
658 Ghan, S. J., Horowitz, L. W., Lee, Y. H., MacKenzie, I. A., Nagashima, T., Naik, V.,
659 Plummer, D., Righi, M., Rumbold, S. T., Schulz, M., Skeie, R. B., Stevenson, D. S., Strode,
660 S., Sudo, K., Szopa, S., Voulgarakis, A. and Zeng, G.: The atmospheric chemistry and climate
661 model intercomparison Project (ACCMIP): Overview and description of models, simulations
662 and climate diagnostics, *Geosci. Model Dev.*, 6(1), 179–206, doi:10.5194/gmd-6-179-2013,
663 2013.
- 664 Law, K. S. and Stohl, A.: Arctic Air Pollution: Origins and Impacts, *Science* (80-.),
665 315(5818), 1537–1540, doi:10.1126/science.1137695, 2007.
- 666 Lelieveld, J., Evans, J. S., Fnais, M., Giannadaki, D. and Pozzer, A.: The contribution of
667 outdoor air pollution sources to premature mortality on a global scale., *Nature*, 525(7569),
668 367–71, doi:10.1038/nature15371, 2015.
- 669 Liu, J., Fan, S., Horowitz, L. W. and Levy, H.: Evaluation of factors controlling long-range
670 transport of black carbon to the Arctic, *J. Geophys. Res.*, 116(D4), D04307,
671 doi:10.1029/2010JD015145, 2011.
- 672 Macdonald, K. M., Sharma, S., Toom, D., Chivulescu, A., Hanna, S., Bertram, A., Platt, A.,
673 Elsasser, M., Huang, L., Chellman, N., McConnell, J. R., Bozem, H., Kunkel, D., Lei, Y. D.,
674 Evans, G. J. and Abbatt, J. P. D.: Observations of Atmospheric Chemical Deposition to High
675 Arctic Snow, *Atmos. Chem. Phys.*, 17, 5775–5788, doi:10.5194/acp-17-5775-2017, 2017.
- 676 McConnell, J. R., Edwards, R., Kok, G. L., Flanner, M. G., Zender, C. S., Saltzman, E. S.,
677 Banta, J. R., Pasteris, D. R., Carter, M. M. and Kahl, J. D. W.: 20th-Century Industrial Black
678 Carbon Emissions Altered Arctic Climate Forcing, *Science* (80-.), 317(5843), 1381–1384,
679 doi:10.1126/science.1144856, 2007.
- 680 Olivier, J. G. J., Aardenne, J. A. Van, Dentener, F. J., Pagliari, V., Ganzeveld, L. N. and
681 Peters, J. A. H. W.: Recent trends in global greenhouse gas emissions: regional trends 1970–
682 2000 and spatial distribution of key sources in 2000, *Environ. Sci.*, 2(2–3), 81–99,



- 683 doi:10.1080/15693430500400345, 2005.
- 684 Petzold, A., Ogren, J. A., Fiebig, M., Laj, P., Li, S. M., Baltensperger, U., Holzer-Popp, T.,
685 Kinne, S., Pappalardo, G., Sugimoto, N., Wehrli, C., Wiedensohler, A. and Zhang, X. Y.:
686 Recommendations for reporting black carbon measurements, Atmos. Chem. Phys., 13(16),
687 8365–8379, doi:10.5194/acp-13-8365-2013, 2013.
- 688 Popovicheva, O. B., Evangelidou, N., Eleftheriadis, K., Kalogridis, A. C., Movchan, V.,
689 Sitnikov, N., Eckhardt, S., Makshtas, A. and Stohl, A.: Black carbon sources constrained by
690 observations and modeling in the Russian high Arctic, Environ. Sci. Technol., submitted,
691 doi:10.1021/acs.est.6b05832, 2017.
- 692 Qi, L., Li, Q., Henze, D. K., Tseng, H.-L. and He, C.: Sources of Springtime Surface Black
693 Carbon in the Arctic: An Adjoint Analysis, Atmos. Chem. Phys. Discuss., (February), 1–32,
694 doi:10.5194/acp-2016-1112, 2017.
- 695 Ruppel, M. M., Isaksson, I., Ström, J., Beaudon, E., Svensson, J., Pedersen, C. A. and
696 Korhola, A.: Increase in elemental carbon values between 1970 and 2004 observed in a 300-
697 year ice core from Holtedahlfonna (Svalbard), Atmos. Chem. Phys., 14(20), 11447–11460,
698 doi:10.5194/acp-14-11447-2014, 2014.
- 699 Sand, M., Berntsen, T. K., von Salzen, K., Flanner, M. G., Langner, J. and Victor, D. G.:
700 Response of Arctic temperature to changes in emissions of short-lived climate forcers, Nat.
701 Clim. Chang., 6(November), 1–5, doi:10.1038/nclimate2880, 2015.
- 702 Seibert, P. and Frank, A.: Source-receptor matrix calculation with a Lagrangian particle
703 dispersion model in backward mode, Atmos. Chem. Phys., 4(1), 51–63, doi:10.5194/acp-4-
704 51-2004, 2004.
- 705 Sharma, S., Ishizawa, M., Chan, D., Lavoué, D., Andrews, E., Eleftheriadis, K. and
706 Maksyutov, S.: 16-year simulation of arctic black carbon: Transport, source contribution, and
707 sensitivity analysis on deposition, J. Geophys. Res. Atmos., 118(2), 943–964,
708 doi:10.1029/2012JD017774, 2013.
- 709 Shiraiwa, M., Kondo, Y., Moteki, N., Takegawa, N., Sahu, L. K., Takami, A., Hatakeyama,
710 S., Yonemura, S. and Blake, D. R.: Radiative impact of mixing state of black carbon aerosol
711 in Asian outflow, J. Geophys. Res. Atmos., 113(24), 1–13, doi:10.1029/2008JD010546, 2008.



- 712 Singh, P. and Haritashya, U. K.: Encyclopedia of Snow, Ice and Glaciers., 2011.
- 713 Slinn, W. G. N.: Predictions for particle deposition to vegetative canopies, Atmos. Environ.,
714 16, 1785–1794, doi:10.1016/0004-6981(82)90271-2, 1982.
- 715 Stein, O., Flemming, J., Inness, A., Kaiser, J. W. and Schultz, M. G.: Global reactive gases
716 forecasts and reanalysis in the MACC project, J. Integr. Environ. Sci., 8168(October 2014),
717 1–14, doi:10.1080/1943815X.2012.696545, 2012.
- 718 Stohl, A., Hittenberger, M. and Wotawa, G.: Validation of the lagrangian particle dispersion
719 model FLEXPART against large-scale tracer experiment data, Atmos. Environ., 32(24),
720 4245–4264, doi:10.1016/S1352-2310(98)00184-8, 1998.
- 721 Stohl, A., Forster, C., Eckhardt, S., Spichtinger, N., Huntrieser, H., Heland, J., Schlager, H.,
722 Wilhelm, S., Arnold, F. and Cooper, O.: A backward modeling study of intercontinental
723 pollution transport using aircraft measurements, J. Geophys. Res. Atmos., 108(D12), 4370,
724 doi:10.1029/2002JD002862, 2003.
- 725 Stohl, A., Forster, C., Frank, A., Seibert, P. and Wotawa, G.: Technical note: The Lagrangian
726 particle dispersion model FLEXPART version 6.2, Atmos. Chem. Phys., 5(9), 2461–2474,
727 doi:10.5194/acp-5-2461-2005, 2005.
- 728 Stohl, A., Andrews, E., Burkhardt, J. F., Forster, C., Herber, A., Hoch, S. W., Kowal, D.,
729 Lunder, C., Mefford, T., Ogren, J. A., Sharma, S., Spichtinger, N., Stebel, K., Stone, R.,
730 Ström, J., Tørseth, K., Wehrli, C. and Yttri, K. E.: Pan-Arctic enhancements of light
731 absorbing aerosol concentrations due to North American boreal forest fires during summer
732 2004, J. Geophys. Res. Atmos., 111(22), 1–20, doi:10.1029/2006JD007216, 2006.
- 733 Stohl, A., Klimont, Z., Eckhardt, S., Kupiainen, K., Shevchenko, V. P., Kopeikin, V. M. and
734 Novigatsky, A. N.: Black carbon in the Arctic: The underestimated role of gas flaring and
735 residential combustion emissions, Atmos. Chem. Phys., 13(17), 8833–8855, doi:10.5194/acp-
736 13-8833-2013, 2013.
- 737 Stohl, A., Aamaas, B., Amann, M., Baker, L. H., Bellouin, N., Berntsen, T. K., Boucher, O.,
738 Cherian, R., Collins, W., Daskalakis, N., Dusinska, M., Eckhardt, S., Fuglestvedt, J. S., Harju,
739 M., Heyes, C., Hodnebrog, Hao, J., Im, U., Kanakidou, M., Klimont, Z., Kupiainen, K., Law,
740 K. S., Lund, M. T., Maas, R., MacIntosh, C. R., Myhre, G., Myriokefalitakis, S., Olivié, D.,
741 Quaas, J., Quennehen, B., Raut, J. C., Rumbold, S. T., Samset, B. H., Schulz, M., Seland,

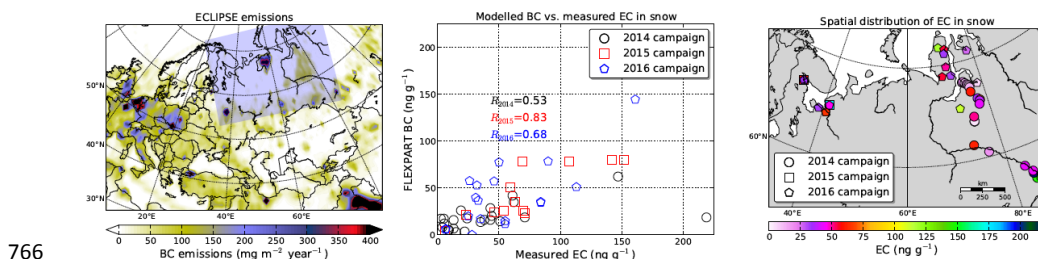


- 742 Shine, K. P., Skeie, R. B., Wang, S., Yttri, K. E. and Zhu, T.: Evaluating the climate and air
743 quality impacts of short-lived pollutants, *Atmos. Chem. Phys.*, 15(18), 10529–10566,
744 doi:10.5194/acp-15-10529-2015, 2015.
- 745 Svensson, J., Ström, J., Hansson, M., Lihavainen, H. and Kerminen, V.-M.: Observed metre
746 scale horizontal variability of elemental carbon in surface snow, *Environ. Res. Lett.*, 8(3),
747 34012, doi:10.1088/1748-9326/8/3/034012, 2013.
- 748 Turner, M. D., Henze, D. K., Capps, S. L., Hakami, A., Zhao, S., Resler, J., Carmichael, G.
749 R., Stanier, C. O., Baek, J., Sandu, A., Russell, A. G., Nenes, A., Pinder, R. W., Napelenok, S.
750 L., Bash, J. O., Percell, P. B. and Chai, T.: Premature deaths attributed to source-specific BC
751 emissions in six urban US regions, , 10(114014), doi:10.1088/1748-9326/10/11/114014/meta,
752 2005.
- 753 Wang, Q., Jacob, D. J., Fisher, J. A., Mao, J., Leibensperger, E. M., Carouge, C. C., Le Sager,
754 P., Kondo, Y., Jimenez, J. L., Cubison, M. J. and Doherty, S. J.: Sources of carbonaceous
755 aerosols and deposited black carbon in the Arctic in winter-spring: Implications for radiative
756 forcing, *Atmos. Chem. Phys.*, 11(23), 12453–12473, doi:10.5194/acp-11-12453-2011, 2011.
- 757 Warren, S. G. and Wiscombe, W. J.: A Model for the Spectral Albedo of Snow. II: Snow
758 Containing Atmospheric Aerosols, *J. Atmos. Sci.*, 37, 2734–2745, doi:10.1175/1520-
759 0469(1980)037<2734:AMFTSA>2.0.CO;2, 1980.
- 760 Winiger, P., Andersson, A., Eckhardt, S., Stohl, A., Semiletov, I. P., Dudarev, O. V., Charkin,
761 A., Shakhova, N., Klimont, Z., Heyes, C. and Gustafsson, Ö.: Siberian Arctic black carbon
762 sources constrained by model and observation, *Proc. Natl. Acad. Sci.*, 1–8,
763 doi:10.1073/pnas.1613401114, 2017.

764



765 **FIGURE CAPTIONS FOR MANUSCRIPT**



766

767 **Figure 1.** Left: Total emissions of BC from the ECLIPSE emission inventory (Klimont et al.,
768 2016). The blue shade shows the area of interest that is zoomed on the right. Middle:
769 Comparison of modelled BC concentrations in snow with measured EC concentrations. Right:
770 Spatial distribution of EC in snow measured by thermal optical analysis (TOA) of filtered
771 snow samples from northwestern European Russia and Western Siberia in spring–time 2014,
772 2015 and 2016.

773

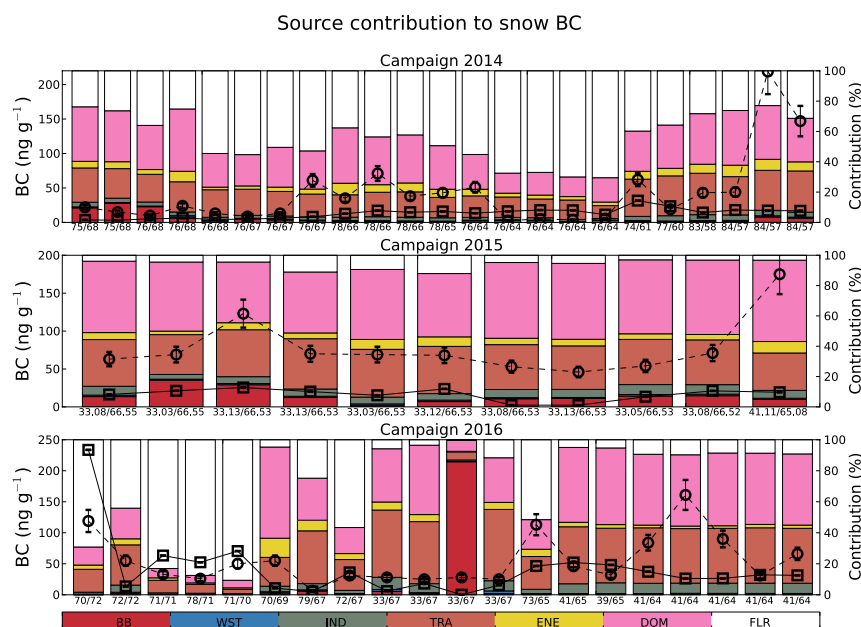
774

775

776

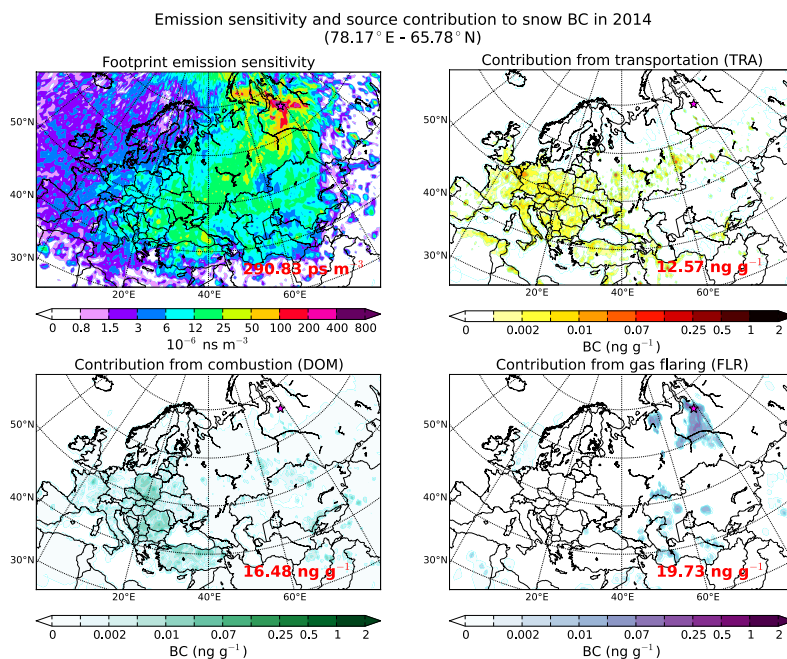
777

778



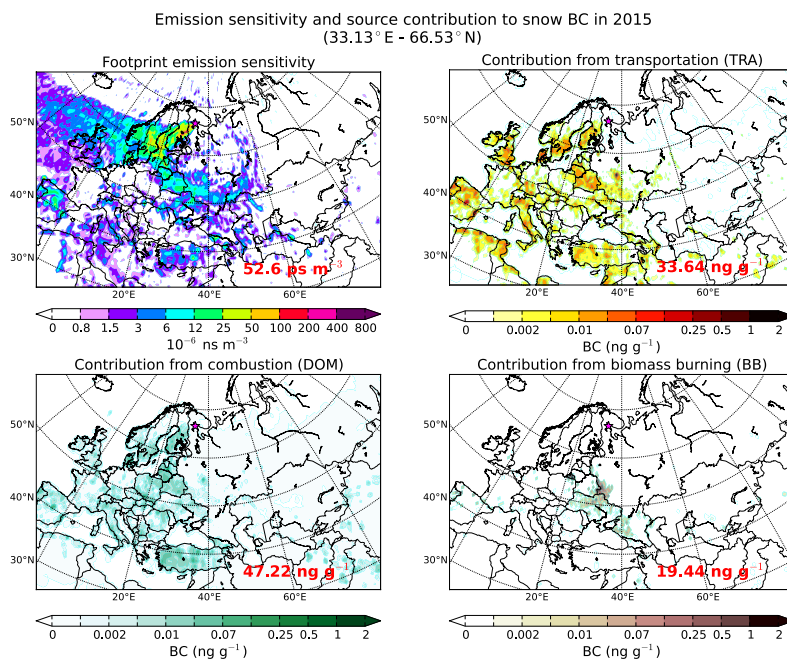
779

780 **Figure 2.** Contribution from the various emission categories considered in the ECLIPSE and
 781 GFED inventories (BB stands for biomass burning, WST for waste burning, IND for
 782 industrial combustion and processing, TRA for surface transportation, ENE for emissions
 783 from energy conversion, and extraction, DOM for residential and commercial combustion,
 784 and FLR for gas flaring) to simulated BC concentrations in snow during the 2014, 2015 and
 785 2016 campaigns in Western Siberia and northwestern European Russia. Bars show the
 786 relative source contribution (0–100%, right axis) and are sorted, from left to right, from the
 787 northernmost to the southernmost measurement location (coordinates are reported on the
 788 bottom as longitude/latitude). Measured EC concentrations in snow are reported with open
 789 circles, whereas modelled BC is shown with open rectangles (left axis).



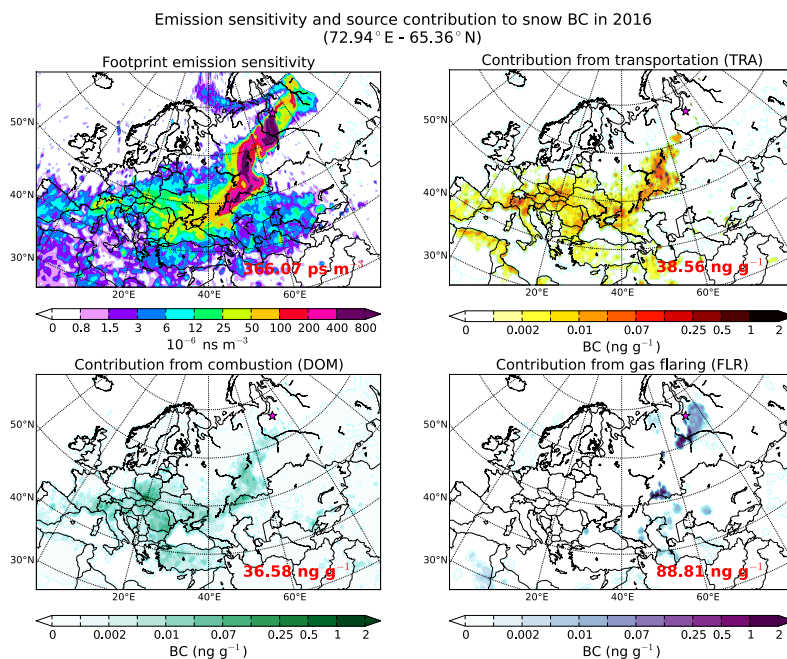
790

791 **Figure 3.** FLEXPART emission sensitivity (top left) and contribution from transportation
 792 (TRA, top right), residential and commercial combustion (DOM, bottom left) and gas flaring
 793 (FLR, top right) to the maximum measured concentration of snow EC recorded along the
 794 transect from Tomsk to Yamal Peninsula in Western Siberia during the campaign of 2014.



795

796 **Figure 4.** FLEXPART emission sensitivity (top left) and contribution from transportation
 797 (TRA, top right), residential and commercial combustion (DOM, bottom left) and gas flaring
 798 (FLR, top right) to the maximum measured concentration of snow EC recorded in
 799 northwestern European Russia (Kindo Peninsula and Arkhangelsk region) during the
 800 campaign of 2015.

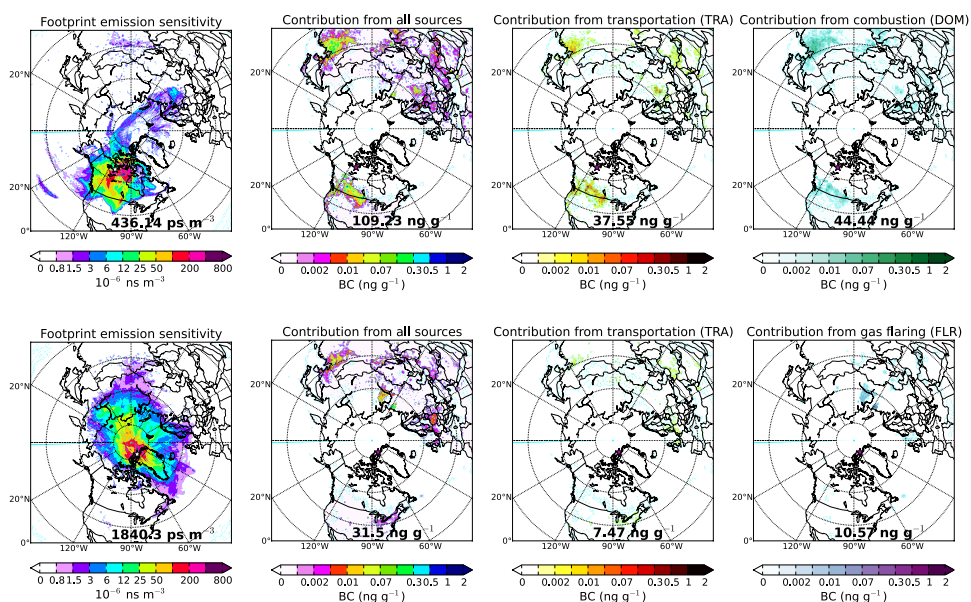


801

802 **Figure 5.** FLEXPART emission sensitivity (top left) and contribution from transportation
 803 (TRA, top right), residential and commercial combustion (DOM, bottom left) and gas flaring
 804 (FLR, top right) to the maximum measured concentration of snow EC recorded in Kindo
 805 Peninsula, Arkhangelsk and Yamal Peninsula (northwestern European Russia, Western
 806 Siberia) during the campaign of 2016.



Emission sensitivity and source contribution to snow BC
(Canadian Arctic 2007 & Alert 2014-2015)



807

808 **Figure 6.** Top row: Footprint emission sensitivity and major contribution from all sources,
 809 TRA and DOM averaged for the samples that showed overestimated modelled concentrations
 810 of BC in 2007 (Doherty et al., 2010). Bottom row: Footprint emission sensitivity and
 811 contribution from all sources, TRA and FLR for the samples collected in Alert (Macdonald et
 812 al., 2017) that model overestimated by more than three times.

813

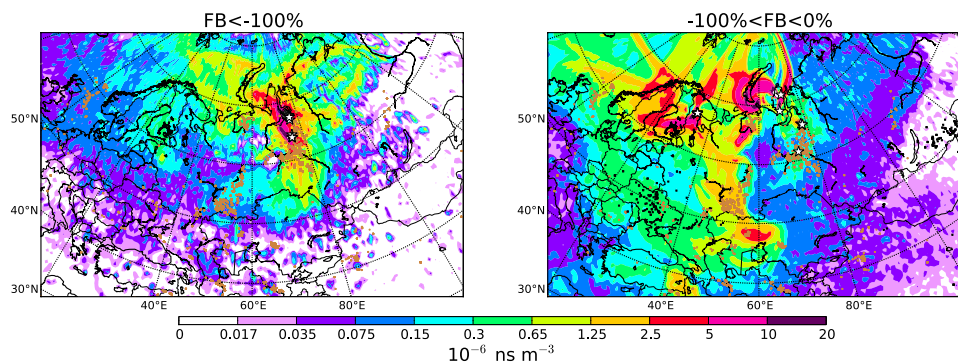
814

815

816



Average footprint emission sensitivities normalised against underestimation from observations



817

818 **Figure 7.** Footprint emission sensitivity from FLEXPART averaged for the sampling points
819 where the model underestimated observations significantly ($FB < -100\%$) and less
820 significantly ($-100\% < FB < 0\%$). Black squares show the locations of active fires
821 detected by MODIS (Moderate Resolution Imaging Spectroradiometer) (Giglio et al., 2003).
822 Brown dots show the location of gas flaring sites from the Global Gas Flaring Reduction
823 Partnership (GGFR) (<http://www.worldbank.org/en/programs/gasflaringreduction>).

824